

## Third-harmonic generation of mode-locked Nd:glass laser pulses in phase-matched Rb-Xe mixtures

H. Puell,\* K. Spanner, W. Falkenstein, and W. Kaiser  
*Physik-Department der Technischen Universität, München, Germany*

C. R. Vidal

*Max-Planck-Institut für Extraterrestrische Physik, Garching, Germany*  
 (Received 5 January 1976; revised manuscript received 7 July 1976)

Third-harmonic generation in phase-matched Rb-Xe mixtures has been produced using 7- and 300-psec pulses of a mode-locked Nd:glass laser with peak powers up to 200 MW. Maximum energy conversion efficiencies of 2.8% have been achieved. A theoretical analysis is given which includes the transient excitations of the system and the linear and nonlinear susceptibilities up to seventh order in the perturbation. Agreement between theory and experiment has been obtained up to the highest input intensities demonstrating the importance of the transient excitation due to the adiabatic following. The phase-matching condition for parallel and focused beams has been investigated showing the influence of density gradients at the boundaries of the nonlinear medium (Rb vapor) and of the field-dependent changes of the refractive index at high input intensities. The limiting processes of self-focusing and multiphoton ionization are discussed.

### I. INTRODUCTION

In recent years it has been demonstrated, in particular, by Harris and co-workers, that alkali-metal vapors have large third-order nonlinear susceptibilities and are well suited for efficient third-harmonic generation and frequency mixing in high-power laser systems.<sup>1,2</sup> This is due to a number of interesting properties:

- (i) Using two-component systems which contain, for example, a mixture of an alkali vapor and a noble gas, phase matching can be achieved by a proper adjustment of the partial pressures, exploiting the anomalous dispersion.<sup>3,4</sup>
- (ii) The third-harmonic generation may be extended to the far-ultraviolet spectral region because of the small continuous photoabsorption cross section.<sup>4</sup>
- (iii) Utilizing the resonant enhancement of the nonlinear susceptibilities, optical mixing of tunable dye-laser radiation becomes very efficient even at moderate laser powers. This technique has been used for the generation of tunable coherent radiation in the range 1600–2000 Å and in smaller frequency intervals at even shorter wavelengths.<sup>5,6</sup>
- (iv) Metal-vapor gas mixtures exposed to the radiation of high-power laser systems are not seriously affected by dielectric breakdown.

Most of the experiments reported so far were performed at rather low laser powers. Using a phase-matched Rb-Xe mixture and a mode-locked Nd:YAG (yttrium aluminum garnet) laser system with a maximum output of 50 kW, Young *et al.*<sup>3</sup> achieved a conversion efficiency for third-harmonic generation of  $5 \times 10^{-8}$ . From the measured nonlinear susceptibility of the Rb vapor they extrapolated a possible conversion efficiency of 50% for an input

power of 10 MW neglecting saturation effects. Very recently, Bloom *et al.*<sup>7</sup> and Puell and Vidal<sup>8</sup> have obtained energy-conversion efficiencies of a few percent in Rb-Xe mixtures, which are the highest values reported so far.

This paper presents experimental results for the third-harmonic generation in Rb-Xe mixtures using incident-light powers up to 200 MW generated by a mode-locked Nd:glass laser system. The experiments have been performed with different durations of the laser pulses (7 and 300 psec) in order to understand the saturation effects observed at high input intensities. A theoretical analysis is given which includes the transient excitations of the system and the various linear and nonlinear susceptibilities up to seventh order. In this manner agreement between theory and experiment has been obtained up to the highest input intensities used in the experiments.

Section II starts with the theory for third-harmonic generation. The influence of focusing, the field-dependent changes of the refractive index, and the influence of excited states due to transient laser excitation are incorporated. Numerical values of the linear and nonlinear susceptibilities are given as required by the experiments. Furthermore, a detailed discussion of the phase-matching condition is given which includes the effect of density gradients at the boundaries of the nonlinear medium. The resulting system of differential equations which describes the third-harmonic generation in a two-component system, has been solved numerically. In Sec. III a description of the experimental arrangement and of the different diagnostics is given. It is followed by a detailed discussion of the experimental results in Sec. IV, which contains the phase-matching curves for a

parallel and a focused beam, the results of the energy conversion for 300- and 7-psec laser pulses and a discussion of the self-focusing and the multiphoton ionization as it applies to the saturation phenomena at high input intensities.

## II. THEORY

### A. Third-harmonic generation

In our analysis of the third-harmonic generation we are interested in the interaction of two linearly polarized electromagnetic waves of frequency  $q\omega$  (with  $q=1$  and  $q=3$ ), allowing for density gradients along the axis of propagation within the nonlinear medium as required by the experiments. We start with the wave equation

$$\Delta \vec{\mathcal{E}}(\vec{r}, t) - \frac{1}{c^2} \frac{\partial^2}{\partial t^2} \vec{\mathcal{E}}(\vec{r}, t) = \frac{4\pi}{c^2} \frac{\partial^2}{\partial t^2} \vec{\mathcal{P}}(\vec{r}, t), \quad (1)$$

where  $\vec{\mathcal{E}}(\vec{r}, t)$  is the total electric field of the two waves,

$$\vec{\mathcal{E}}(\vec{r}, t) = \frac{1}{2} \sum_{q=1,3} \vec{E}_q(\vec{r}, t) e^{-iq\omega t} + \text{c.c.}, \quad (2)$$

and  $\vec{\mathcal{P}}(\vec{r}, t)$  is the total polarization induced in the nonlinear medium by this field, which may be calculated according to the results of the preceding paper.<sup>9</sup> It is convenient to separate the Fourier components of the polarization  $\vec{P}_q$  into a linear term  $\vec{P}_q^L$  and two nonlinear terms  $\vec{P}_q^T$  and  $\vec{P}_q^S$ :

$$\vec{\mathcal{P}}(\vec{r}, t) = \frac{1}{2} \sum_{q=1,3} \left( \vec{P}_q^L(\vec{r}, t) + \vec{P}_q^T(\vec{r}, t) + \vec{P}_q^S(\vec{r}, t) \right) e^{-iq\omega t} + \text{c.c.} \quad (3)$$

Generally, the linear polarization  $\vec{P}_q^L$  is expressed in terms of the field-independent linear susceptibility  $\chi^{(1)}(q\omega)$ ,

$$\vec{P}_q^L(\vec{r}, t) = N \chi^{(1)}(q\omega) \vec{E}_q(\vec{r}, t), \quad (4)$$

with

$$\chi^{(1)}(q\omega) = \sum_m \frac{|\mu_{m0}|^2}{\hbar} \left( \frac{1}{q\omega - \omega_{0m}} - \frac{1}{q\omega - \omega_{m0}} \right). \quad (5)$$

$N$  is the number of atoms per unit volume in the initially populated energy level 0. For our experimental situation, where the frequencies  $q\omega$  are far away from any atomic transition frequency of Rb and the pulse duration  $\tau$  is short compared to the energy relaxation time  $T_1$ , only those results of Ref. 9 are used which have been derived for the so-called "off-resonance" case with  $|q\omega - \omega_{mn}| \gg 1/\tau \gg 1/T_1$ . The transition frequencies  $\omega_{mn}$  between the eigenstates  $E_m$  and  $E_n$  of the medium are given in a complex notation:

$$\omega_{mn} = (E_m - E_n)/\hbar - i\Gamma_{mn} = \Omega_{mn} - i\Gamma_{mn}, \quad (6)$$

where the relaxation term  $\Gamma_{mn}$  represents for  $m \neq n$  the phase relaxation rate and for  $m = n$  the energy relaxation rate.  $|\mu_{mn}|$  is the corresponding dipole-moment matrix element of the transition.

The real part of  $\chi^{(1)}(q\omega)$  is related to the refractive index  $n_q$  of the medium by

$$n_q^2 - 1 = 4\pi N \text{Re}[\chi^{(1)}(q\omega)], \quad (7)$$

whereas the imaginary part represents the linear power absorption coefficient

$$\tilde{\alpha}_q = \frac{4\pi q\omega}{cn_q} \text{Im}[\chi^{(1)}(q\omega)]. \quad (8)$$

The nonlinear polarization  $P_q^T$  represents the polarization induced in the medium due to the interaction of the two waves under consideration. Going up to the third order of the perturbation one obtains

$$\begin{aligned} \vec{P}_1^T(\vec{r}, t) &= \frac{1}{4} N \chi^{(3)}(\omega = 3\omega - \omega - \omega) \\ &\quad \times \vec{E}_3(\vec{r}, t) \vec{E}_1^*(\vec{r}, t) \vec{E}_1^*(\vec{r}, t) \end{aligned} \quad (9)$$

and

$$\begin{aligned} \vec{P}_3^T(\vec{r}, t) &= \frac{1}{4} N \chi^{(3)}(3\omega = \omega + \omega + \omega) \\ &\quad \times \vec{E}_1(\vec{r}, t) \vec{E}_1(\vec{r}, t) \vec{E}_1(\vec{r}, t), \end{aligned} \quad (10)$$

where both third-order susceptibilities are related by<sup>10</sup>

$$\chi_T^{(3)}(3\omega) \equiv \chi^{(3)}(3\omega = \omega + \omega + \omega) = \frac{1}{3} \chi^{(3)}(\omega = 3\omega - \omega - \omega). \quad (11)$$

The third term  $P_q^S$  in Eq. (3) describes the mutual interaction of the incident and the generated light waves giving rise to an intensity dependence of the refractive indices at the frequencies  $\omega$  and  $3\omega$  (second-order Kerr effect). Evaluating  $P_q^S$  also up to the third order of the perturbation we obtain

$$\begin{aligned} \vec{P}_1^S &= \frac{1}{4} N [\chi^{(3)}(\omega = \omega + \omega - \omega) |\vec{E}_1|^2 \vec{E}_1 \\ &\quad + \chi^{(3)}(\omega = \omega + 3\omega - 3\omega) |\vec{E}_3|^2 \vec{E}_1] \end{aligned} \quad (12)$$

and

$$\begin{aligned} \vec{P}_3^S &= \frac{1}{4} N [\chi^{(3)}(3\omega = 3\omega + 3\omega - 3\omega) |\vec{E}_3|^2 \vec{E}_3 \\ &\quad + \chi^{(3)}(3\omega = 3\omega + \omega - \omega) |\vec{E}_1|^2 \vec{E}_3]. \end{aligned} \quad (13)$$

From symmetry considerations the four nonlinear susceptibilities may be reduced to three independent coefficients which will be abbreviated in the following as

$$\chi_S^{(3)}(q\omega) \equiv \chi^{(3)}(q\omega = q\omega + q\omega - q\omega), \quad (14)$$

with  $q=1$  and  $q=3$ , and

$$\begin{aligned}\chi_S^{(3)}(\omega, 3\omega) &\equiv \chi^{(3)}(\omega = \omega + 3\omega - 3\omega) \\ &= \chi^{(3)}(3\omega = 3\omega + \omega - \omega).\end{aligned}\quad (15)$$

All the third-order nonlinear susceptibilities may be evaluated from time-dependent perturbation theory.<sup>9</sup> Numerical values for a fundamental wavelength of  $\lambda = 1.06 \mu\text{m}$  are presented in Table I. Performing these calculations for Rb we used the same energy levels and the multiplet splitting, and the same values for the reduced dipole matrix elements as previously employed by Eicher,<sup>11,12</sup> who calculated the  $\chi_R^{(3)}(3\omega)$  coefficient for the ground state of all the alkali metals.

Here we should point out that all the susceptibilities are identical with the values obtained from stationary perturbation theory<sup>10,11</sup> although our experiments were performed in the transient region with  $\tau \ll T_1$ . This is due to incorporating the transient virtual excitations, as shown in detail in Ref. 9.

Comparing the numerical values in Table I we find that the  $\chi_S^{(3)}(3\omega)$  and the  $\chi_S^{(3)}(\omega, 3\omega)$  coefficients may be neglected in our further discussion of the third-harmonic generation. The influence of the higher-order susceptibilities, namely, the fifth order, will be shown in the Appendix.

We now proceed with the solution of Eq. (1). Since we are interested in the interaction of focused light beams we describe the Fourier components of the electric field amplitude by the field distribution of a Gaussian beam (TEM<sub>00</sub> mode) propagating along the  $z$  direction,<sup>13</sup>

$$\vec{E}_q(\vec{r}, t) = \hat{E}_q(r, z, t) A_q(r, z) e^{ik_q z}, \quad (16)$$

with

$$\begin{aligned}A_q(r, z) &= (1 + i2z/b)^{-1} \exp[-k_q r^2 / (b + i2z)] \\ &= F^{-1/2} G_q e^{-i\delta_q}.\end{aligned}\quad (17)$$

For a linear medium,  $\hat{E}_q(r, z, t)$  is a constant in space and time and represents the maximum field amplitude within the focal plane ( $z = 0$ ) of the wave with frequency  $q\omega$  and wave vector  $k_q$ . [Note that  $\vec{r}$  is the vector to point  $(x, y, z)$ , whereas  $r$  is the radial coordinate in the plane perpendicular to the  $z$  axis.] Owing to the nonlinear interaction with the medium, however, the amplitude  $\hat{E}_q(r, z, t)$  becomes space and time dependent. This dependence

has to be maintained explicitly to account for distortions of the Gaussian beam. The confocal parameter  $b$  is given by  $b = 2k_q R_q^2$ , where  $R_q$  is the  $1/e$  radius of the intensity distribution within the focal plane.  $F(z) = 1 + (2z/b)^2$  represents the cross section of the light beam at a distance  $z$ , normalized to the focal-spot size, and  $G_q = \exp(-k_q r^2 / bF)$  specifies the Gaussian radial intensity distribution. Finally,  $\delta_q$  represents the phase shift associated with the focusing,

$$\delta_q = \arctan(2z/b) + (2z/b) \ln G_q. \quad (18)$$

Inserting Eqs. (2), (3), and (16) into Eq. (1) and taking into account the slow-amplitude approximation

$$\left| \frac{\partial^2}{\partial z^2} \right| \ll k_q \left| \frac{\partial}{\partial z} \right|, \quad \left| \frac{\partial^2}{\partial t^2} \right| \ll (q\omega)^2$$

and the fact that  $A_q(r, z)$  satisfies the equation<sup>14</sup>

$$\left( \Delta_{\perp} + 2ik_q \frac{\partial}{\partial z} \right) A_q(r, z) = 0,$$

we obtain for the amplitudes of the Fourier component with frequency  $q\omega$  traveling in a medium which shows density gradients along the direction of propagation  $z$ ,

$$\begin{aligned}\frac{d\hat{E}_q}{dz} + iz\hat{E}_q \frac{dk_q}{dz} - \frac{i}{k_q A_q} \left( \frac{A_q}{2} \Delta_{\perp} \hat{E}_q + \nabla_{\perp} A_q \cdot \nabla_{\perp} \hat{E}_q \right) \\ = i \frac{2\pi (q\omega)^2}{c^2 k_q A_q} (\vec{P}_q^T + \vec{P}_q^S) e^{-ik_q z} - \frac{\tilde{\alpha}_q}{2} \hat{E}_q,\end{aligned}\quad (19)$$

where  $\Delta_{\perp}$  and  $\nabla_{\perp}$  are the two-dimensional Laplace operators in the plane perpendicular of the  $z$  axis. Equation (19) represents a set of coupled differential equations, since the nonlinear polarizations  $\vec{P}_q^T$  given by Eqs. (9) and (10) are functions of different Fourier components  $\hat{E}_q$ . The second term in Eq. (19) represents the phase shift of the amplitude  $\hat{E}_q$  associated with the  $z$ -dependent refractive index, due to the assumed density gradients. (The intensity dependence of the refractive index is incorporated within the nonlinear polarization  $\vec{P}_q^S$ ). The third term in Eq. (19), containing the transverse Laplace operators  $\Delta_{\perp}$  and  $\nabla_{\perp}$ , describes the mutual interaction of the changes in the radial phase and intensity distributions, which are normalized with respect to a focused Gaussian beam defined by  $A_q$ . This term is important for the problem of self-focusing.<sup>15</sup> In the following, however, it will be neglected, which is a good approximation as long as radial phase variations remain small.

Equation (19) may now be applied to the problem of third-harmonic generation. Making use of Eqs. (9)–(11), (16), and (17) the electric fields  $\hat{E}_1$  and  $\hat{E}_3$  with the frequencies  $\omega$  and  $3\omega$  are given by

TABLE I. Third-order nonlinear susceptibilities (esu) for the 5S ground state of Rb calculated for  $\lambda = 10\,600 \text{ \AA}$  as defined by Eq. (11), (14), and (15).

$\chi_T^{(3)}(3\omega)$	$\chi_S^{(3)}(\omega)$	$\chi_S^{(3)}(3\omega)$	$\chi_S^{(3)}(\omega, 3\omega)$
$8.56 \times 10^{-33}$	$2.41 \times 10^{-31}$	$3.57 \times 10^{-34}$	$-9.94 \times 10^{-34}$

$$\frac{d\hat{E}_1^*}{dz} = -i \frac{2\pi\omega^2}{c^2 k_1} \left( \frac{3N}{4F} \chi_T^{(3)}(3\omega) \hat{E}_1^2 \hat{E}_3^* G_1 G_3 \exp[i(\Delta k z + \delta_3 - 3\delta_1)] + \frac{e^{i k_1 z} P_1^{S*}}{A_1^*} \right) - \frac{\alpha_1}{2} \hat{E}_1^* + i z \hat{E}_1^* \frac{dk_1}{dz}, \quad (20)$$

$$\frac{d\hat{E}_3}{dz} = i \frac{2\pi 9\omega^2}{c^2 k_3} \left( \frac{N}{4F} \chi_T^{(3)}(3\omega) \hat{E}_1^3 \frac{G_3}{G_1} \exp[i(\Delta k z + \delta_3 - 3\delta_1)] + \frac{e^{-i k_3 z} P_3^S}{A_3} \right) - \frac{\alpha_3}{2} \hat{E}_3 - i z \hat{E}_3 \frac{dk_3}{dz}, \quad (21)$$

where we used the notation

$$\Delta k = 3k_1 - k_3 = (3\omega/c)(n_1 - n_3). \quad (22)$$

Equations (20) and (21) give a detailed description of the third-harmonic generation by a focused light beam, including the phase variations due to the self-action of the light beams  $P^S$  and the density gradients along the  $z$  axis. The influence of the changes in phase on the beam propagation, which leads to self-focusing, is not included in our subsequent considerations. A more detailed discussion of this effect will be given in Sec. IV. It should be repeated that the amplitudes  $\hat{E}_1$  and  $\hat{E}_3$  in Eqs. (20) and (21) are space and time dependent. In the small-signal limit, where this dependence may be neglected (together with the self-action  $P^S$ ), we find the third-harmonic emission to remain a Gaussian beam; for  $\Delta k \ll k_1, k_3$  and  $G_1^3/G_3 \approx 1$ , Eq. (21) contains no radial dependence any more.<sup>13</sup> Since we are mainly interested in situations where the phase-matching condition is closely satisfied, the factor  $G_1^3/G_3$  is neglected in our subsequent calculations.

Before rewriting Eqs. (20) and (21) in a convenient form for numerical computation, let us discuss the small-signal approximation ( $E_3 \ll E_1$ ). Neglecting the self-action  $P^S$  and the absorption coefficient  $\alpha_q$ , and introducing the intensity  $\hat{\Phi}_q = n_q c |E_q|^2 / 8\pi$ , we get from Eq. (21) for the third-harmonic intensity  $\Phi_3$  generated in a nonlinear homogeneous medium ( $dk_q/dz = 0$ ) of length  $L = z_2 - z_1$ ,

$$\hat{\Phi}_3 = (4\pi^2 k_3 N / c)^2 (n_1 n_3)^{-3} |\chi_T^{(3)}(3\omega)|^2 \hat{\Phi}_1^3 |I(\Delta k, z, b)|^2, \quad (23)$$

where

$$\begin{aligned} I(\Delta k, z, b) &= \int_{z_1}^{z_2} \frac{1}{F} \exp[i(\Delta k z + \delta_3 - 3\delta_1)] dz \\ &= \int_{z_1}^{z_2} \frac{e^{i\Delta k z}}{(1 + i2z/b)^2} dz \end{aligned} \quad (24)$$

is identical with the phase-matching integral given by Ward and New,<sup>16</sup> and Bjorklund.<sup>17</sup> For plane waves ( $b \rightarrow \infty$ ) Eq. (23) yields the known expression for the small-signal third-harmonic intensity,

$$\begin{aligned} \hat{\Phi}_3 &= \left( \frac{4\pi^2 k_3 N}{c} \right)^2 (n_1 n_3)^{-3} |\chi_T^{(3)}(3\omega)|^2 \\ &\quad \times \hat{\Phi}_1^3 L^2 \left( \frac{\sin(\Delta k L / 2)}{\Delta k L / 2} \right)^2. \end{aligned} \quad (25)$$

In order to obtain the third-harmonic power  $W_3$  in terms of the fundamental power  $W_1$ , Eq. (25) may readily be integrated over the spatial coordinates, with the result

$$\begin{aligned} W_3 &= \frac{1}{3} \left( \frac{4\pi k_3 N}{c R_1^2} \right)^2 (n_1 n_3)^{-3} |\chi_T^{(3)}(3\omega)|^2 \\ &\quad \times W_1^3 L^2 \left( \frac{\sin(\Delta k L / 2)}{\Delta k L / 2} \right)^2. \end{aligned} \quad (26)$$

Assuming a Gaussian time dependence for the fundamental power,  $W_1(t) = W_1 e^{-t^2/\tau^2}$ , the third-harmonic energy  $\mathcal{J}_3$  is given by integrating Eq. (26),

$$\begin{aligned} \mathcal{J}_3 &= \frac{\pi}{3\sqrt{3}} \left( \frac{4k_3 N}{c R_1^2 \tau} \right)^2 (n_1 n_3)^{-3} |\chi_T^{(3)}(3\omega)|^2 \\ &\quad \times \mathcal{J}_1^3 L^2 \left( \frac{\sin(\Delta k L / 2)}{\Delta k L / 2} \right)^2. \end{aligned} \quad (27)$$

Returning to the general solution of Eqs. (20) and (21), which includes depletion of the fundamental wave due to the harmonic generation and the phase shifts associated with the second-order Kerr-effect and the density gradients, we separate the two equations into their real and imaginary parts.<sup>10</sup> Writing  $\hat{E}_q(r, z, t) = \rho_q(r, z, t) e^{i\varphi_q(r, z, t)}$  and

$$\Theta = \varphi_3 - 3\varphi_1 - z\Delta k(z) - (\delta_3 - 3\delta_1), \quad (28)$$

we get the following system of differential equations:

$$\frac{d\rho_1}{dz} = -\frac{3\pi\omega}{2n_1 c F} N \chi_T^{(3)}(3\omega) \rho_1^2 \rho_3 G_1 G_3 \sin\Theta, \quad (29)$$

$$\frac{d\rho_3}{dz} = \frac{3\pi\omega}{2n_3 c F} N \chi_T^{(3)}(3\omega) \rho_1^3 \sin\Theta, \quad (30)$$

$$\begin{aligned} \frac{d\Theta}{dz} &= \frac{3\pi\omega}{2n_1 c F} N \left[ \chi_T^{(3)}(3\omega) \rho_1 \left( \frac{n_1}{n_3} \frac{\rho_1^2}{\rho_3} - 3G_1 G_3 \rho_3 \right) \cos\Theta \right. \\ &\quad \left. - \text{Re}[\chi_S^{(3)}(\omega)] \rho_1^2 G_1^2 \right] - \Delta k(z) + \frac{4}{bF}. \end{aligned} \quad (31)$$

Equations (29) and (30) describe the depletion of the fundamental wave and the generation of the

third harmonic, respectively, neglecting any attenuation due to absorption processes. The third-order susceptibility  $\chi_T^{(3)}(3\omega)$  was assumed to be a real quantity. If the imaginary part is not sufficiently small, as in case of resonant enhancement, a second term proportional to  $\cos\Theta$  has to be added to Eqs. (29) and (30). Equation (31) describes the change of the phase difference of both waves. Note that  $\Delta k(z)$  varies along the  $z$ -axis owing to the assumed density gradients. In evaluating  $d\Theta/dz$ , however, the term  $z d\Delta k/dz$  is cancelled by an identical term originating from  $d(\varphi_3 - 3\varphi_1)/dz$ .

According to Eq. (30) the largest growth rate of the third-harmonic wave is given for  $\Theta = \pi/2$ . In this case the first term of Eq. (31) disappears and the angle  $\Theta$  can only be maintained if all the remaining terms of Eq. (31) vanish. This result is an extension of the usual phase-matching condition and includes the terms  $\Delta k - 4/bF$  and the influence of the field-dependent second-order Kerr effect. (The Kerr constant for the third-harmonic frequency,  $\chi_s^{(3)}(3\omega)$ , and  $\chi_s^{(3)}(\omega, 3\omega)$  were neglected.) A more detailed discussion will be given in Sec. II B. It should be noted that for exact phase matching the angle  $\Theta = \pi/2 + 2n\pi$  is the only stable one, because any other angle will immediately lead to a change of phase, due to the first term in Eq. (31), until  $\Theta = \pi/2 + 2n\pi$ . Only in this case is a complete conversion of the fundamental wave into the third-harmonic wave possible.

Equations (29)–(31) provide a complete set of differential equations describing the third-harmonic generation in a nonlinear medium for arbitrary field amplitudes. For a comparison with our experimental results we integrated this system numerically with respect to time (assuming a Gaussian time dependence of the fundamental wave) and space ( $z$  axis), taking into account the radial intensity distribution  $G_q$ . The initial conditions were chosen to be  $\rho_3(t=0) = 0$ ,  $\Theta(t=0) = \pi/2$ , and all the atoms of the nonlinear medium are in the ground state.

In our experiments the fundamental frequency is far from any one- or two-photon resonance. In this case real populations of excited states as well as the corresponding attenuation of the fundamental wave can be neglected. For the near-resonance case, where this simplification is no longer valid, the contributions of the excited states to the Eqs. (29)–(31) may be included via a system of rate equations for the population of the excited states considering the linear and nonlinear susceptibilities as a superposition of the contributions due to all the different populated states.

The results of our numerical calculations are presented in Sec. IV and will be discussed further

in Sec. V. In Sec. II B the phase-matching condition and the influence of inhomogeneities at the boundaries of the nonlinear medium are discussed.

### B. Phase matching

For efficient third-harmonic generation it is important to consider the phase-matching condition which is determined by Eq. (31). In the small-signal limit we find that the wave-vector mismatch  $\Delta k$  is compensated to some extent by the phase shift  $4/bF$  due to focusing. Hence, we expect optimum phase matching, i.e., optimum output, to occur at some positive value of  $\Delta k$ . The situation is simplified even further in the limit of plane waves, where  $4/bF = 0$ . According to Eq. (25) the harmonic intensity is then proportional to the third power of the fundamental intensity and the square of the "phase-matching factor"  $\sin(\Delta k L/2)/(\Delta k L/2)$ , which becomes unity for  $\Delta k = 3k_1 - k_3 = 0$  and decreases rapidly with increasing mismatch.

In the case of harmonic generation in crystals the phase-matching condition is generally achieved by making use of the birefringence of the crystals.<sup>18</sup> In liquids or gases one may take advantage of the anomalous dispersion.<sup>10,19</sup> Young *et al.*<sup>3</sup> have shown that phase matching at  $\lambda_1 = 10\,640$  Å and  $\lambda_3 = 3547$  Å may be obtained in a mixture of Rb vapor and xenon. Owing to the resonance transition of Rb at  $\lambda_0 = 7948$  Å, the metal vapor has a larger refractive index at the fundamental wave than at the third harmonic, whereas for xenon the opposite is true. In Ref. 3 perfect phase matching was reported for a pressure ratio  $p_{Xe}/p_{Rb} = 410$ . Theoretically the mixing ratio is calculated from the relation

$$\Delta k = 3k_1 - k_3 = (3\omega/c)(n_1 - n_3) = 0, \quad (22)$$

where  $n_1$  and  $n_3$  are the indices of refraction at the fundamental and the harmonic frequency, respectively. Since the refractive index of a gas is not very different from unity, we write for  $n_q$  in a Rb-Xe mixture

$$n_q \simeq 1 + 2\pi \{ N_{Rb} \text{Re}[\chi_{Rb}^{(1)}(q\omega)] + N_{Xe} \text{Re}[\chi_{Xe}^{(1)}(q\omega)] \}, \quad (32)$$

where  $N_{Rb}$  and  $N_{Xe}$  are the number density of the respective gases. With Eq. (22) one immediately obtains the phase-matching ratio

$$\left(\frac{N_{Xe}}{N_{Rb}}\right)_0 = \frac{\text{Re}[\chi_{Rb}^{(1)}(\omega) - \chi_{Rb}^{(1)}(3\omega)]}{\text{Re}[\chi_{Xe}^{(1)}(3\omega) - \chi_{Xe}^{(1)}(\omega)]} \quad (33)$$

and the mismatch for a given density or pressure ratio,

TABLE II. Linear susceptibilities of Rb and Xe, pressure ratios for perfect phase matching, and the constant  $D$  defined in Eq. (36) calculated for the wavelengths of the Nd:glass laser (10 600 Å) and of the Nd:YAG laser (10 640 Å).

$\lambda$ (Å)	$\text{Re}[\chi_{\text{Rb}}^{(1)}(\lambda)]$ ( $\times 10^{-22}$ )	$\text{Re}[\chi_{\text{Rb}}^{(1)}(\lambda/3)]$ ( $\times 10^{-23}$ )	$\text{Re}[\chi_{\text{Xe}}^{(1)}(\lambda)]$ ( $\times 10^{-24}$ )	$\text{Re}[\chi_{\text{Xe}}^{(1)}(\lambda/3)]$ ( $\times 10^{-24}$ )	$\left(\frac{N_{\text{Xe}}}{N_{\text{Rb}}}\right)_0$	$D$ ( $\times 10^{-19}$ )
10 600	1.04	-1.39	4.0498	4.3695	369.8	-3.572
10 640	1.03	-1.45	4.0495	4.3664	372.2	-3.559

$$\Delta k = \frac{3\omega}{c} 2\pi [\chi_{\text{Xe}}^{(1)}(\omega) - \chi_{\text{Xe}}^{(1)}(3\omega)] N_{\text{Rb}} \left[ \frac{N_{\text{Xe}}}{N_{\text{Rb}}} - \left( \frac{N_{\text{Xe}}}{N_{\text{Rb}}} \right)_0 \right] = D \left[ N_{\text{Xe}} - N_{\text{Rb}} \left( \frac{N_{\text{Xe}}}{N_{\text{Rb}}} \right)_0 \right]. \quad (34)$$

Values for the phase-matching ratio and for the constant  $D$  are given in Table II for the wavelength of the Nd:glass laser (10 600 Å) and the Nd:YAG laser (10 640 Å). In addition, numerical values for the linear susceptibilities of Rb and Xe are presented. The values for xenon were obtained from a formula for the refractive index of xenon given by Koch.<sup>20</sup>

There is a difference in the phase-matching ratio reported by Young *et al.* and our calculated value. We suspect that this discrepancy is due to the difficulty of measuring the partial pressure of Rb, if one relies on temperature measurements and vapor-pressure curves. Furthermore, the optimum phase-matching ratio is intensity dependent, as shown below, and only in the small-signal limit will the ratio given in Table II be observed.

According to Eq. (25) the harmonic intensity is a periodic function of  $\Delta k L/2$  centered symmetrically around  $\Delta k = 0$ , implying a homogeneous medium of length  $L$  with sharp boundaries. This is generally true for crystals or liquids and gases bounded by windows. If the metal vapor is prepared in a heat pipe,<sup>21</sup> we have transition zones at the end of the vapor column,<sup>22</sup> the width of which depends in a complicated manner on the thermal conductivity, particle diffusion, and structure of the heat pipe. Using our computer program for evaluating Eqs. (29)–(31) the influence of such density gradients on the shape of the phase-matching curve was investigated. These calculations have been carried out in the small-signal limit for a parallel incident light beam ( $b = \infty$ ). The density distribution of the Rb vapor was approximated by

$$N_{\text{Rb}} \approx \frac{1}{2} N [1 + \tanh(\alpha L/2 - \alpha |z|)], \quad (35)$$

where  $N$  is the Rb density at the center of the heat-pipe oven. As long as the condition  $1/\alpha \ll L/2$  holds, the total number of Rb atoms per  $\text{cm}^2$  is identical to the number contained in a homogeneous

column of length  $L$ .

The results of our numerical calculations for different values of  $\alpha$  are shown in Fig. 1, where the harmonic energy normalized to the third power of the fundamental energy is given as a function of the xenon pressure. The partial pressure of Rb at  $z = 0$  is assumed to be 1 Torr. The upper scale gives the corresponding mismatch  $\Delta k$  according to Eq. (34). The particle density  $N$  has been determined from the pressure  $p$  by means of the ideal gas law  $p = NkT$ , with  $T = 568^\circ\text{K}$  being the temperature at a vapor pressure of 1 Torr. The length of the nonlinear medium was chosen to be  $L = 28$  cm, similar to our experimental conditions in Sec. IV.

Figure 1 reveals two important features: (a) For a rectangular density distribution ( $\alpha = \infty$ ) we get the usual symmetric phase-matching curve [Eq. (25)]. As the density gradients decrease the phase-matching curve becomes more and more asymmetric. The secondary maxima on the low-pressure side ( $\Delta k > 0$ ) increase, whereas those on the high-pressure side decrease. For very small gradients there are no additional maxima for  $\Delta k$

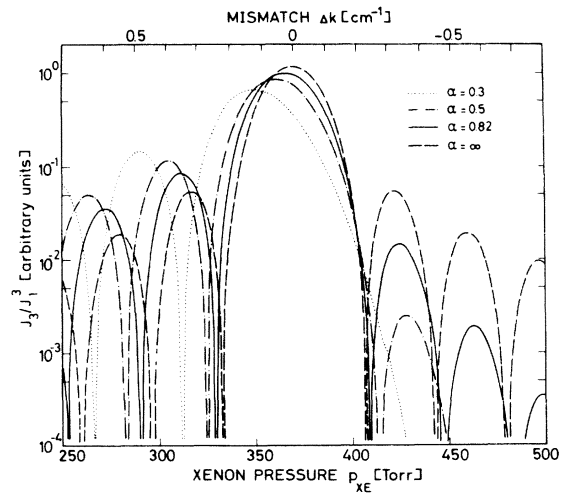


FIG. 1. Third-harmonic energy  $J_3$  normalized with respect to  $J_1^3$  as a function of the Xe pressure for 1-Torr Rb, a length of the nonlinear medium  $L = 28$  cm, and different density gradients  $\alpha$ . The corresponding mismatch  $\Delta k$  is shown at the top.

$< 0$ . (b) With decreasing density gradients the optimum phase-matching pressure ratio is shifted from  $\Delta k = 0$  to positive values of  $\Delta k$ .

The interpretation of these results is straightforward. In a Xe-Rb mixture with a partial pressure of Xe smaller than the optimum phase-matching value, there will always be a range within the transition zones (characterized by the density gradient  $\alpha$ ) where the condition  $\Delta k = 0$  holds. These zones contribute significantly to the harmonic output. On the other hand, for a Xe partial pressure higher than the optimum value, the condition  $\Delta k = 0$  is never achieved. In Sec. IV an experimental verification of these results will be given.

The preceding considerations have been carried out in the small-signal limit. At high input intensities the phase matching is significantly influenced by intensity-dependent changes of the refractive index, which are incorporated in Eq. (31). At very high input intensities its influence on the phase difference  $\Theta$  eventually starts to dominate and destroys the phase-matching condition, since different radial regions within the fundamental beam experience different phase shifts. It should be noted that the latter effect is explicitly taken into account in our numerical evaluation of Eqs. (29)–(31) by integrating over time and space as explained above.

### III. EXPERIMENTAL ARRANGEMENT

A schematic of the experimental set up for investigating the third-harmonic generation in a Rb-Xe gas mixture is shown in Fig. 2. The Nd:glass laser system consists of a mode-locked oscillator, a single-pulse selector, and several amplifier stages. During the course of our experiments two different oscillator configurations were used: (i) a hemispherical resonator formed by two (wedged) dielectric mirrors M1 and M2 with radii of curvature  $R = 10$  m and  $R = \infty$ , and reflectivities of 99.8% and 50%, respectively; (ii) a nearly confocal resonator, where the mirror M2 was replaced by a (wedged) dielectric mirror with  $R = 3$  m and 50% reflectivity. In both cases the active medium was a 20-cm-long Nd:glass rod. A dye cell DC filled with Kodak 9740 Q-switch solution was used for mode locking. Laser rod and switching dye were placed at Brewster's angle within the resonator.

A single light pulse was selected from the pulse train by a fast electro-optic shutter<sup>23</sup> consisting of a Kerr cell KC placed between two crossed polarizers PO and activated by a laser-triggered spark gap SG. After passing the beam expander BE the selected light pulse was amplified by the following amplifier system (Nd:glass rods A1–A4, 30 cm long, 10–16-mm diameter). For optical isolation

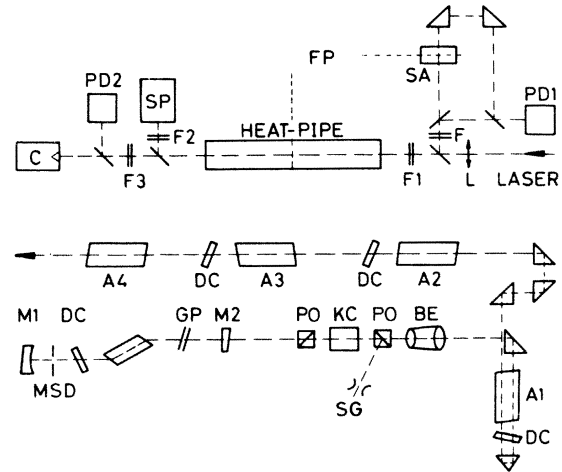


FIG. 2. Schematic of the experimental arrangement. The lower half shows the mode-locked oscillator, the electro-optic shutter for single-pulse operation, and the amplifier stages. The upper half contains the heat-pipe system and the diagnostics consisting of fast photodiodes, filters, a pyroelectric energy meter, a saturable absorber, and a spectrometer.

saturable absorbers DC were placed between the different amplifier stages.

The output of this laser system was carefully investigated with respect to pulse duration and radial intensity distribution. Using the resonator configuration 1 and inserting two plane parallel glass plates GP (1 and 1.1 mm in thickness) for mode selection, we generated single pulses with an energy content up to 30 mJ (measured with a calibrated pyroelectric energy meter) and a pulse duration of  $\tau_H \approx 300$  psec ( $\tau_H$  is the full half-width measured by the two-photon fluorescence method<sup>24</sup>). TEM<sub>00</sub>-mode operation was possible without inserting the transversal mode-selecting diaphragm MSD when operating the oscillator very close to its threshold. The gain of the amplifier system was adjusted in such a manner that the Gaussian output pattern of the oscillator was not significantly distorted. (At high output energies of 1 J the intensity distribution became irregular.)

The resonator configuration 2 was operated without the (longitudinal) mode-selecting glass plates GP in order to get very short mode-locked pulses. TEM<sub>00</sub>-mode operation was ensured by inserting the (transversal) mode-selecting diaphragm MSD of 2-mm diameter. This system was operated with the last two amplifier stages removed. Single light pulses were generated with energies up to 5 mJ, a pulse duration of  $\tau_H \approx 7$  psec, and a Gaussian intensity distribution.

The output of the laser system was focused by a lens L (focal length  $f = 200$  cm) into the center of a

concentric heat-pipe oven<sup>21</sup> containing a homogeneous mixture of Rb vapor and xenon gas. The concentric heat-pipe system allows an independent and accurate determination of the partial pressures  $p_{\text{Rb}}$  and  $p_{\text{Xe}}$  without relying on vapor-pressure curves. The total pressure of the outer heat pipe is equal to  $p_{\text{Rb}}$  and the total pressure of the inner heat pipe gives the value of  $p_{\text{Rb}} + p_{\text{Xe}}$ . Using two commercial capacitive manometers, the ratio  $p_{\text{Xe}}/p_{\text{Rb}}$  may easily be measured with an accuracy of better than 1%.

During the experiment great care was taken to monitor the incoming laser energy and the light intensity within the focal plane. For this purpose a small portion of the incoming focused light beam was sent through a nonlinear absorber SA placed in the focal plane FP of lens L. Recording the incident and the transmitted energy with the calibrated fast photodiode PD1 we were able to determine the input energy and— from the transmission of the saturable absorber<sup>25</sup>—the light intensity within the focal plane. Independently, the light intensity was determined from the experimentally measured values of the pulse energy (photodiode PD1), pulse duration (two-photon fluorescence), and the focal-spot diameter  $2R$ . The latter quantity was estimated from the beam divergence (in the far field), using the relation  $2R = f\epsilon$ . The two resonator configurations used in our experiments showed different beam divergences ( $\epsilon_1 = 2.2 \times 10^{-4}$  rad and  $\epsilon_2 = 1.9 \times 10^{-4}$  rad). The corresponding cross section of the focal spots were  $F_1 = 1.5 \times 10^{-3}$  cm<sup>2</sup> and  $F_2 = 1.1 \times 10^{-3}$  cm<sup>2</sup>. The intensity values derived in this way ( $\hat{\Phi} \approx J/F\tau_H$ ) agreed quite well with the nonlinear-absorber measurements. Therefore, during the course of the experiments, the readily measured input energy was monitored as the relevant quantity, whereas the saturable-absorber method was used to check the consistency of our input laser parameters.

The third-harmonic light generated within the heat pipe was recorded with a calibrated pyroelectric detector C (sensitive down to  $2 \mu\text{J}$ ) and a fast photodiode PD2. Calibration of this diode was performed by recording the 10-mJ output of third-harmonic light generated in two ADP crystals simultaneously with the calorimeter and the photodiode. The fundamental wave was blocked by the filter set F3. Furthermore, a small portion of the light transmitted by the heat pipe was deflected to a quartz spectrograph for analyzing its spectral properties. Our diagnostics covered all experimental parameters required for a comparison of our experiment with theory, except for the length  $L$  of the nonlinear medium. This parameter depends strongly on the pressure inside the heat pipe oven and on the applied heating power. It cannot

easily be determined since lateral observation of the Rb column is not possible. Using the blue emission of an argon-ion laser the red, laser-induced resonance fluorescence of the  $\text{Rb}_2$  molecules was observed. In this way the vapor zone was estimated to have a total length  $L \approx 30$  cm. A more accurate value of  $L$  can be deduced from the measured phase-matching curve as described in Sec. IV.

#### IV. EXPERIMENTAL RESULTS

The main purpose of our experimental work was to investigate the efficiency of third-harmonic generation at high input intensities. For a quantitative analysis of the different nonlinear processes we started with a parallel light beam at low power levels and investigated the phase-matching conditions of the Rb-Xe mixture. We then increased the input intensity by focusing the laser output into the nonlinear medium. The new phase-matching curve resulting from the focused beam was determined. Finally, the generated harmonic energy was measured over five orders of magnitude as a function of incident energy at different values of the Rb-Xe pressure ratio. These measurements were performed with two different pulse durations in order to discriminate between different nonlinear processes which might be responsible for the conversion saturation observed at high input intensities.

##### A. Phase matching

The first experiments were performed with a parallel light beam with a cross section of  $0.086$  cm<sup>2</sup>, a pulse duration of  $300$  psec (oscillator configuration 1), and a energy content of  $0.025$  J. Keeping the input intensity of  $\sim 10^9$  W/cm<sup>2</sup> and the Rb pressure of  $1$  Torr constant, the generated third-harmonic energy was monitored as a function of the Xe pressure. In Fig. 3 the results are presented. The measured third-harmonic energy was normalized with respect to the third power of the fundamental energy in order to compare our measurements with the phase-matching factor  $[\sin(\Delta kL/2)/(\Delta kL/2)]^2$  according to Eq. (27). The upper scale, indicating the mismatch  $\Delta k$  for a given Rb-Xe pressure ratio, was obtained from Eq. (34). Our experimental results show two interesting features: The phase-matching curve is clearly asymmetric with respect to the amplitudes of the side maxima and the optimum phase matching occurs at about  $\Delta k = +0.03$  cm<sup>-1</sup>.

Equation (27) predicted a symmetric curve centered around  $\Delta k = 0$ , as indicated by the dashed curve, which was computed from Eq. (27) for a

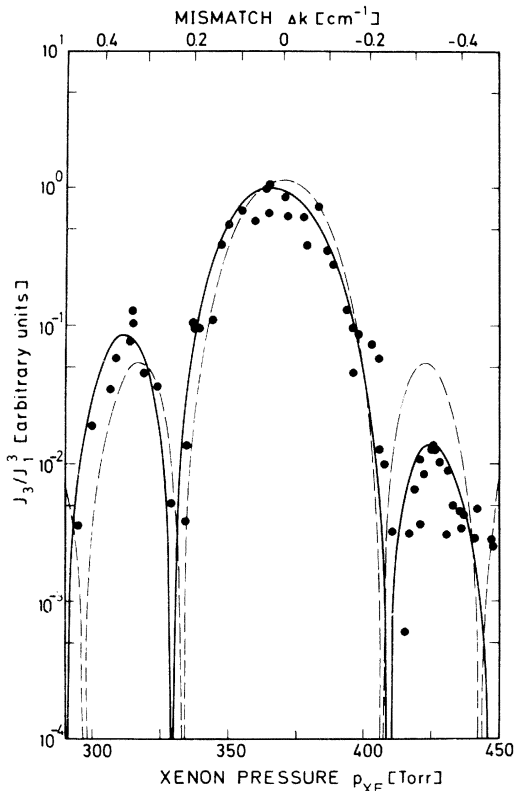


FIG. 3. Phase-matching curve for a parallel beam ( $p_{\text{Rb}}=1$  Torr,  $L=28$  cm). The theoretical curves for different density gradients of the metal vapor in the heat pipe are shown. [ $\alpha=\infty$  (broken line) and  $\alpha=0.82$  cm $^{-1}$  (solid line).]

length  $L=28$  cm of the (homogeneous) nonlinear medium. This value of  $L$  is deduced with good accuracy from the position of the well-established minima of the generated third-harmonic energy, where  $\Delta kL/2$  becomes equal to multiples of  $\pi$ . Taking into account the influence of the density gradients as shown in Fig. 1, an excellent fit of our experimental data was obtained for  $\alpha=0.82$  cm $^{-1}$  (solid line). This value, which corresponds to a density increase from 10 to 90% within a length of 4 cm, is reasonable for a metal vapor prepared in a heat-pipe oven.<sup>22</sup>

It should be noted that initially our fitting procedure indicated a displacement of the  $\Delta k$  scale by 0.06 cm $^{-1}$ . Since the position and the shape of the phase-matching curve is accurately fixed by the value  $\alpha$  of the density gradient and the length  $L$  of the medium we concluded that the observed additional displacement of 0.03 cm $^{-1}$  is due to an uncertainty of the matrix elements required for the calculation of the linear susceptibilities of Rb. The susceptibility of Xe was interpolated from experimental data,<sup>20</sup> whereas the values for Rb are

based on semiempirical calculations of the oscillator strengths.<sup>11,26</sup> Lowering the absolute value of the reduced dipole-moment matrix element for the dominant 5S-5P transition by only 1% from 5.31 to 5.25 a.u., gives excellent agreement between experiment and theory. In Fig. 3 the upper scale was evaluated from Eq. (34) using this new value for the dipole moment of the resonance transition. A modification of the linear susceptibility of Xe is not justified, because the accuracy of the measurements of Koch<sup>20</sup> is certainly better than 1%. This discussion shows that the phase-matching curve is a powerful method for the accurate determination of relative oscillator strengths as long as the pressure ratios are measured with good accuracy.

For an input energy of 25 mJ and optimum phase matching we observed a generated third-harmonic energy of  $2.7 \times 10^{-4}$  mJ, which is close to the theoretical value of  $3.2 \times 10^{-4}$  mJ calculated from Eqs. (29)–(31) for a nonlinear medium of  $L=28$  cm and  $\alpha=0.82$  cm $^{-1}$ . At the maximum output of our laser system (30 mJ) a conversion efficiency of  $2 \times 10^{-5}$  was obtained with the parallel light beam.

In a second experiment the laser output was focused into the heat pipe with a  $f=200$ -cm lens. The resulting decrease of the beam diameter to 0.44 mm within the focal plane (confocal parameter  $b=57$  cm) provided an intensity increase of a factor of 56. With this experimental arrangement we measured again the phase-matching curve at low input energies ( $\approx 3$  mJ) and low Rb vapor pressure (0.35 Torr). The results are plotted in Fig. 4 in the same way as discussed in connection with Fig. 3. Since the Rb pressure was lower by a factor of 3, the heating power of the heat-pipe oven had to be reduced in order to obtain a length of the nonlinear medium similar to that used in the previous experiments. The length  $L$  was determined again from the phase-matching curve looking for the best fit of our numerical calculations. A value of  $L=35$  cm is deduced from the data of Fig. 4.

As expected from theory, the optimum wave-vector mismatch was shifted by  $4/b=0.07$  cm $^{-1}$ , resulting from the focused beam, and in addition by a value of 0.03 cm $^{-1}$ , due to the density gradient  $\alpha=0.82$  cm $^{-1}$ . The value of  $\alpha$  was assumed to be unaffected by the slightly different heating power supplied to the heat-pipe oven. The experimentally measured third-harmonic energy of  $1.3 \times 10^{-4}$  mJ at  $\Delta k=0.1$  cm $^{-1}$  for an input energy of 2.5 mJ was again in good agreement with the numerically calculated value of  $1.2 \times 10^{-4}$  mJ.

For comparison, the calculated phase-matching curve for a parallel beam with a beam diameter equal to the focal-spot diameter passing through

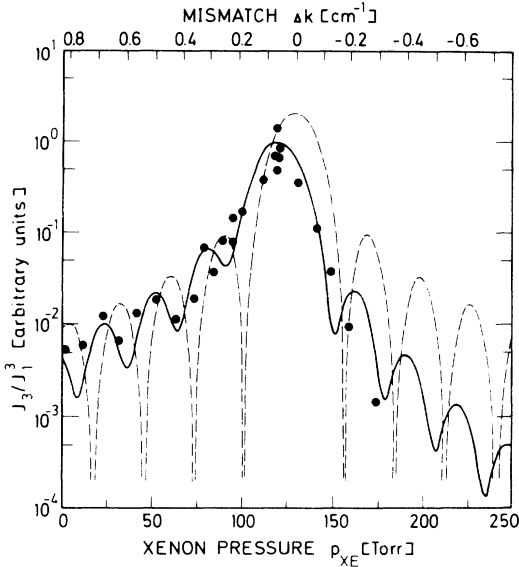


FIG. 4. Phase-matching curve for a focused beam ( $b = 57$  cm,  $p_{Rb} = 0.35$  Torr,  $L = 35$  cm). Two theoretical curves for different density gradients of the metal vapor in the heat pipe are shown. [ $\alpha = \infty$  (broken line) and  $\alpha = 0.82$  cm $^{-1}$  (solid line).]

a homogeneous Rb vapor column of 35-cm length is plotted in Fig. 4 (dashed curve). It is interesting to note that in the case of focusing the minima are much less pronounced, in agreement with experimental observations. The different radial regions of the focused light beam see different optical path lengths, and the condition  $\Delta kL = n\pi$  is not fulfilled for all radial regions simultaneously.

The experimental results reported so far have shown that for low input intensities, where the second-order Kerr effect may be neglected, the third-harmonic generation in Rb-Xe mixtures is in good agreement with theory. This confirms the numerical value of the nonlinear susceptibility  $\chi_r^{(3)}(3\omega)$  for the ground state of Rb shown in Table I. In addition, some important system parameters, such as length and density gradients of the medium, have been accurately measured which so far have never been determined independently. We now proceed to the investigation of the third-harmonic generation at higher input intensities up to  $2 \times 10^{11}$  W/cm $^2$ .

#### B. Energy dependence for 300-psec pulses

Using laser pulses of a duration of 300 psec we investigated the third-harmonic generation as a function of the input energy  $J_1$  for different Rb pressures near optimum phase matching. The results are shown in Fig. 5, where the third-harmonic intensity  $\hat{\Phi}_3$  is plotted versus the input

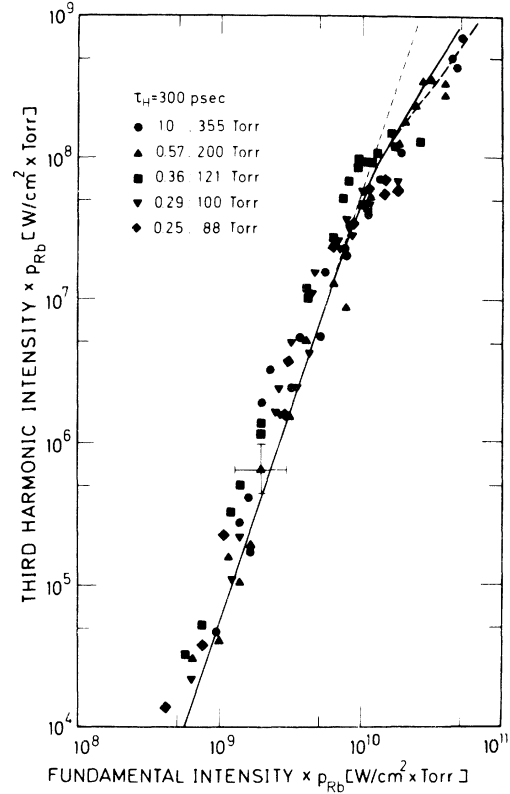


FIG. 5. Plot of the third-harmonic intensity times Rb vapor pressure,  $\hat{\Phi}_3 p_{Rb}$ , versus input intensity times Rb vapor pressure,  $\hat{\Phi}_1 p_{Rb}$  ( $\tau_H = 300$  psec,  $L = 28$  cm). Theoretical curves are given for the small-signal limit (dashed line), for the third-order calculation including the second-order Kerr effect (broken line), and for the fifth-order calculation (solid line).

intensity  $\hat{\Phi}_1$  normalized with respect to the partial pressure  $p_{Rb}$  of Rb. Introducing the new variables  $N^{1/2} \rho_1$  and  $N^{1/2} \rho_3$ , Eqs. (29)–(31) become independent of the particle density  $N$ . Hence, a plot  $p_{Rb} \hat{\Phi}_3$  versus  $p_{Rb} \hat{\Phi}_1$  holds in general for all values of  $p_{Rb}$  as long as the initial mismatch  $\Delta k$  remains the same.

The photodiodes monitoring the harmonic and fundamental output give energy values. Conversion to intensity is performed according to  $\Phi = J/F\tau_H$ , assuming a Gaussian temporal and radial intensity distribution, as discussed in Sec. III. Converting the third-harmonic energy values to intensity values, the cross section and the pulse duration have been reduced by a factor of 3 and  $\sqrt{3}$ , respectively. This procedure is valid for all our measurements for which the depletion of the fundamental electric field amplitude is negligible and the radial distortion of the harmonic beam due to intensity-dependent phase matching is insignificant.

The fundamental intensity was varied between

$5 \times 10^8$  and  $5 \times 10^{10}$  W/cm<sup>2</sup>. At input powers below  $10^{10}$  W/cm<sup>2</sup> the third-harmonic intensity increases over nearly four orders of magnitude proportional to the third power of the fundamental intensity, as expected from theory. Furthermore, our experimental results verify the theoretical pressure dependence of the third harmonic,  $\Phi_3 \propto p_{\text{Rb}}^2$ . Our data points for the different Rb pressures follow, within the accuracy of our measurements, the same line in the normalized plot. It should be noted that the experiments with different pressures were not performed under identical conditions with respect to the length and the initial mismatch of the system. According to Eq. (34)  $\Delta k$  varied from  $0.09$  cm<sup>-1</sup> for  $p_{\text{Rb}} = 1$  Torr to  $0.027$  cm<sup>-1</sup> for  $p_{\text{Rb}} = 0.25$  Torr. The length  $L$  was determined from the phase-matching curves, as described above, and varied from  $L = 28$  cm for  $p_{\text{Rb}} = 1$  Torr to  $L = 35$  cm for  $p_{\text{Rb}} = 0.36$  Torr. Consequently, small systematic deviations of the experimental results from the straight line are expected for the different pressures. The calculated corrections are small compared to the scatter of our data points. The latter is mainly due to the shot-to-shot variation of the pulse duration and of the focal-spot diameter, and the accuracy of the energy measurements of  $\pm 10\%$ , indicated by the error bars.

For low input intensities our experimental results are in good quantitative agreement with theory, as can be seen by comparison with the dashed curve (which coincides with the solid line in the low-intensity region). This curve was calculated from Eqs. (29)–(31) with  $\chi_r^{(3)}(3\omega) = 8.6 \times 10^{-33}$  esu and our experimental parameters:  $\Delta k = 0.09$  cm<sup>-1</sup>,  $L = 28$  cm,  $b = 57$  cm,  $p_{\text{Rb}} = 1$  Torr =  $1.7 \times 10^{16}$  cm<sup>-3</sup>; the second order Kerr-effect was neglected.

At input intensities above  $10^{10}$  W/cm<sup>2</sup> a significant discrepancy between our experimental data and the small-signal theory is observed. For  $5 \times 10^{10}$  W/cm<sup>2</sup>, for example, one would expect a third-harmonic intensity of  $6 \times 10^9$  W/cm<sup>2</sup>, whereas experimentally  $7 \times 10^8$  W/cm<sup>2</sup> have been measured. This effect cannot be attributed to a depletion of the fundamental beam. The experimentally measured transmission of the fundamental wave through the nonlinear medium indicated a negligible attenuation. This observation is expected, since at  $5 \times 10^{10}$ -W/cm<sup>2</sup> input intensity the conversion to the third harmonic amounts to  $10^{-3}$ . The onset of other nonlinear processes, such as parametric amplification<sup>27</sup> (which grow at the expense of the third-harmonic generation), may be ruled out because of the spectral analysis of the outgoing light beam. Only the frequencies of the fundamental and the third-harmonic waves were found on photographic recordings of the spectrum

from 3000 to 11 000 Å. In the infrared spectral region from 1.1 to 3.0  $\mu\text{m}$  we used a PbS photo-resistor with a Si window, 5 mm in thickness, blocking all the radiation with  $\lambda < 1.1$   $\mu\text{m}$ . No radiation in the infrared was detected.

We believe that the deviations of our experimental data from the dashed curve in Fig. 4 have to be attributed to an intensity-dependent change of the phase-matching condition. Miles and Harris<sup>2</sup> have discussed this effect for a number of alkali-vapor-noble-gas mixtures; they give approximate values of the maximum fundamental light intensity for which no significant change of the phase-matching condition occurs. Since we have calculated different numbers, their analysis is not applied to our experiments.

Our system of differential equations describing the third-harmonic generation, Eqs. (29)–(31), include the second-order Kerr effect. We are able to compute the third-harmonic output under given experimental conditions. The results of these calculations are shown in Fig. 5.

The broken curve in Fig. 5 represents the theoretical third-harmonic intensity, taking into account the second-order Kerr effect with  $\chi_s^{(3)}(\omega) = 2.4 \times 10^{-31}$  esu (see Table I). As a result, good agreement between theory and experiment is observed. A careful analysis of the numerical solutions reveals that the decrease is due to changes of the phase-matching condition. For  $5 \times 10^{10}$  W/cm<sup>2</sup>, for instance, the second-order Kerr effect changes the refractive index for the fundamental wave in such a way that the wave-vector mismatch increases from  $\Delta k = 0.09$  cm<sup>-1</sup> (given by the Rb-Xe pressure ratio) to  $\Delta k = 0.55$  cm<sup>-1</sup>.

The rather pronounced influence of the second-order Kerr effect on the conversion efficiency at high input intensities strongly suggests that even higher-order nonlinearities have to be considered. For this purpose Eqs. (29)–(31) have been extended to fifth order, as shown in the Appendix. Integrating Eqs. (A11)–(A13) yields the solid line in Fig. 5, which is calculated for a pressure ratio  $p_{\text{Rb}}/p_{\text{Xe}} = (1.0 \text{ Torr})/(355 \text{ Torr})$ . For the data points taken at other pressures the theoretical curve in our normalized plot has to be slightly modified at the highest input intensities because the density normalization is no longer fully appropriate for the fifth-order correction terms. One realizes that up to input intensities of  $5 \times 10^{10}$  W/cm<sup>2</sup> the fifth-order terms give rise only to a minor modification which is still well within the error bars of our measurements.

### C. Energy dependence for 7-psec pulses

Third-harmonic generation at even higher input intensities was investigated with the oscillator

configuration 2 delivering 7-psec light pulses. With this system we were able to generate light intensities up to  $2 \times 10^{11}$  W/cm<sup>2</sup> within the focal plane of lens L (see Fig. 2). The slightly different beam divergence of the laser system gave a confocal parameter  $b = 43$  cm and a focal spot diameter of 0.038 cm. Length and density gradients of the nonlinear medium remained at  $L = 28$  cm and  $\alpha = 0.82$  cm<sup>-1</sup>, respectively.

Keeping the Rb and the Xe pressure at 1 and 372 Torr, respectively, the generated third-harmonic energy was recorded as a function of the input energy. The results are presented in Fig. 6. In addition, the results of numerical calculations are shown. The dashed curve corresponds again to the solution of Eqs. (29)–(31) neglecting the second-order Kerr effect. For “low” input intensities ( $5 \times 10^9$  to  $5 \times 10^{10}$  W/cm<sup>2</sup>) an increase of the third-harmonic intensity is observed which follows approximately the third power of the incident intensity, whereas at higher intensities again a significant deviation from this power law is noticed.

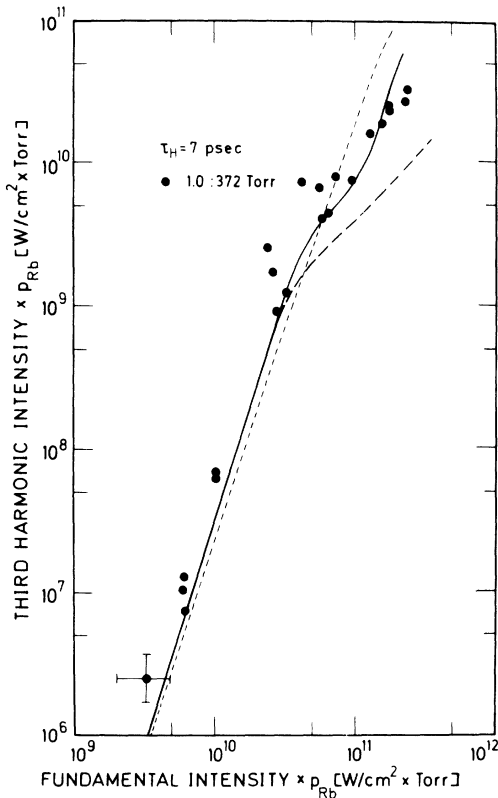


FIG. 6. Plot of the third-harmonic intensity times Rb vapor pressure,  $\Phi_3 p_{Rb}$ , versus input intensity times Rb vapor pressure,  $\Phi_1 p_{Rb}$  ( $\tau_H = 7$  psec,  $L = 28$  cm). Theoretical curves are given for the small-signal limit (dashed line), for the third-order calculation (broken line), and for the fifth-order calculation (solid line).

At an input intensity of  $2 \times 10^{11}$  W/cm<sup>2</sup>, for instance, one expects from the small-signal theory (dashed curve) a third-harmonic intensity of  $10^{11}$  W/cm<sup>2</sup>, which has to be compared with the measured value of  $2.5 \times 10^{10}$  W/cm<sup>2</sup>. Note that the dashed curve begins to saturate for input intensities greater  $10^{11}$  W/cm<sup>2</sup> because the fundamental wave is depleted at the expense of the third-harmonic wave. Such a depletion does not appear to be the origin for the saturation observed experimentally, since it becomes effective for energy conversions above typically 5%; the highest energy conversion observed in our experiment was 2.8%.

If we now incorporate in our calculations the field-dependent change of the refractive index due to the second-order Kerr effect  $\chi_S^{(3)}(\omega)$ , one obtains the broken curve in Fig. 6. Contrary to our measurements carried out with the 300-psec laser pulses one recognizes a severe discrepancy at high input intensities. This is primarily due to the different initial pressure ratio which was chosen for reasons explained below.

Similar to the experiments of Sec. IV B, the calculations were extended to fifth order, giving rise to the solid line of Fig. 6. A rather satisfactory agreement is obtained. One may wonder whether in this case even higher-order nonlinearities have to be considered. That this is not the case is demonstrated in Table III, which shows for the highest input intensity of  $2 \times 10^{11}$  W/cm<sup>2</sup> the calculated energy-conversion efficiency, adding from one line to the next the indicated nonlinear coefficients. One realizes that the most severe changes occur owing to the third- and fifth-order field-dependent corrections of the refractive index,  $\chi_S^{(3)}(\omega)$  and  $\chi_S^{(5)}(\omega)$ . It is also clear from Table III that seventh-order corrections may be neglected. They have

TABLE III. Calculated energy-conversion efficiency for an input intensity of  $2 \times 10^{11}$  W/cm<sup>2</sup>, incorporating the indicated nonlinear susceptibilities in successive order.

	Energy conversion (%)
$\chi_T^{(3)}(3\omega)$	8.71
$\chi_S^{(3)}(\omega)$	0.77
Total 3rd order	0.77
$\chi_T^{(5)}(3\omega)$	0.96
$\chi_S^{(5)}(\omega)$	4.98
Total 5th order	4.10
$\chi^{(1)}(4D)$	4.18
$\chi_T^{(7)}(3\omega)$	4.37
$\chi_S^{(7)}(\omega)$	4.37
$\chi^{(3)}(4D)$	4.43

been calculated with  $\chi_T^{(2)}(3\omega) = 3.5 \times 10^{-50}$  esu and  $\chi_S^{(2)}(\omega) = -6.9 \times 10^{-50}$  esu.

As already indicated the Rb system shows no close one- or two-photon resonances for the 1.06- $\mu\text{m}$  radiation of the Nd:glass laser. For this reason we have so far neglected any real excitations and have restricted our analysis to the transient processes. In order to justify this approach we investigated the influence of a real population of the 4D level, which shows the best resonance condition with respect to the ground state (the two-photon transition 5S-4D is 487- $\text{cm}^{-1}$  off-resonance). A contribution of this kind can be noticed in fifth order as an additional polarization proportional to  $E \int E^4 dt$ , which may be interpreted as a contribution of the 4D-level population to the refractive index.<sup>9</sup> Similarly, one obtains in seventh order an additional polarization proportional to  $E^3 \int E^4 dt$ , which may now be interpreted as a contribution of the 4D-level population to the third-order nonlinear susceptibilities. Terms of this kind, which in a simplified notation are abbreviated by  $\chi^{(1)}(4D)$  and  $\chi^{(3)}(4D)$ , have been included in our calculations and the results are given in Table III. It is apparent that a real population of the 4D level has no influence on the energy-conversion efficiency within the range of our measurements. The reason for this is that the linear and third-order nonlinear susceptibilities of the 4D level are very close to the corresponding values of the ground state. In addition, even for input intensities of  $2 \times 10^{11}$  W/cm<sup>2</sup> one only obtains typical population densities of about 1%.

The preceding calculations have clearly demonstrated that the saturation in the third-harmonic generation at high input intensities is dominated by the breaking of the phase-matching condition due to the field-dependent changes of the refractive indices. The loss of phase matching at high power levels can be reduced by properly adjusting the Rb-Xe pressure ratio. Since the third-harmonic generation is a highly nonlinear process the dominant contribution results from the peak intensity of the fundamental wave. A considerable increase in conversion efficiency is expected when the pressure ratio is adjusted in such a way as to compensate the intensity-dependent changes of the refractive index at the moment of the maximum intensity.

This idea is demonstrated by numerical calculations of the phase-matching curves for low and high input energies, as shown in Fig. 7. The numerical values for the parameters used in these computations correspond to our experimental situation with the 7-psec pulses. For an input energy of 0.0087 mJ, corresponding to an input intensity of  $10^9$  W/cm<sup>2</sup>, one obtains a phase-matching

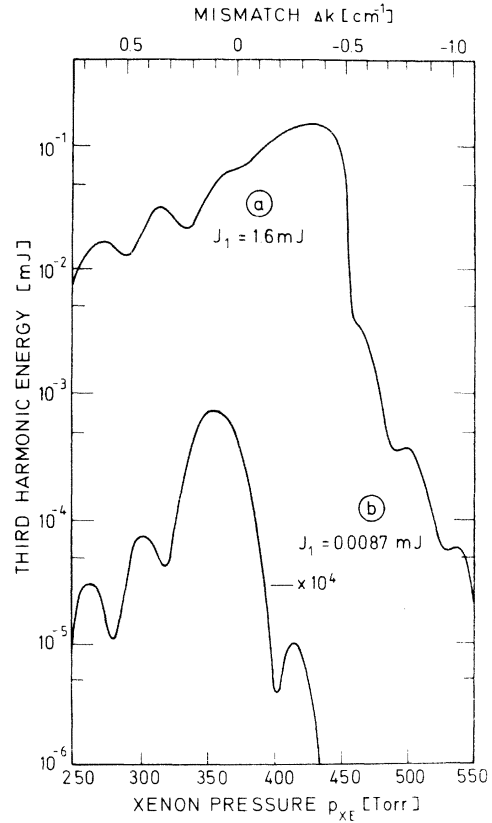


FIG. 7. Theoretical phase-matching curves for focused beams ( $b = 43$  cm,  $\tau_H = 7$  psec,  $L = 28$  cm) with input energies of  $J_1 = 0.087$  mJ (line b, small-signal approximation) and  $J_1 = 1.74$  mJ (line a), respectively. Note line b was multiplied by factor  $10^4$ . The high-energy case shows the drastic influence of the different nonlinearities.

curve centered around  $\Delta k = 0.1$   $\text{cm}^{-1}$  (pressure ratio 1:355), according to the small-signal limit. As indicated above the small shift with respect to  $\Delta k = 0$  and the pronounced asymmetry is due to the focused beam and the density gradients. At a much larger input energy of 1.6 mJ, corresponding to an intensity of  $2 \times 10^{11}$  W/cm<sup>2</sup>, the optimum phase matching occurs at  $\Delta k = -0.37$   $\text{cm}^{-1}$  (pressure ratio 1:430) and the oscillations are washed out. Note that the energy conversion at optimum phase matching amounts to 10%, which has to be compared with the theoretical value of 4.1% and the experimental value of 2.8% at  $\Delta k \approx 0$ .

#### D. Self-focusing

So far we have considered only the influence of the intensity-dependent refractive index on the phase-matching condition. However, it is well known that the nonlinear refractive index  $n_2$  acts

also on the wave propagation: Positive or negative values of  $n_2$  lead to self-focusing or defocusing of the light beam, respectively. This effect is not included in our theoretical treatment of the third-harmonic generation, since in all the equations following Eq. (19) we neglected the radial derivatives of the complex field amplitude  $\hat{E}$ , which effectively decouples the different radial regions of the incoming beam. In this way one retains the information about the radial variation of the field amplitude [included in  $G_q(r, z)$ ], but loses the phase information, which describes the distortion of the wave fronts and, hence, self-focusing or defocusing effects. The solution of the wave equation (19) including these effects is quite complicated and out of the scope of this paper. We will restrict our discussion to an estimate of the power level at which self-focusing becomes important for our experimental results.

The critical power  $W_{cr}$ , for which the focusing due to the (positive) nonlinear refractive index  $n_2$  overcomes the diffractive divergence of the light beam, is given by<sup>15</sup>

$$W_{cr} = (1.22\lambda)^2 c / 256n_2, \quad (36)$$

where  $n_2$  is defined as an expansion coefficient of the total refractive index,

$$n = n_0 + n_2 |E|^2 + n_4 |E|^4 + \dots \quad (37)$$

Hence,  $n_2$  includes all the terms which contribute to a polarization  $P(\omega)$  proportional to  $E^3$ ; i.e.,  $n_2$  is proportional to the real part of the third-order nonlinear susceptibility  $\chi_S^{(3)}(\omega)$ :

$$n_2 = \frac{N}{n_0} \frac{\pi}{2} \chi_S^{(3)}(\omega). \quad (38)$$

Inserting the numerical values for  $\chi_S^{(3)}(\omega)$  given in Table I we get  $n_2 \approx (3.8 \times 10^{-31}) N \text{esu}$ , where  $N$  is the number density of Rb atoms. Inserting this value into Eq. (36) we find for a Rb pressure of 1 Torr ( $N = 1.7 \times 10^{16} \text{cm}^{-3}$ ) a critical power of  $W_{cr} \approx 3 \times 10^7 \text{W}$ .

The critical power may be modified owing to the higher-order expansion coefficients in Eq. (37). The coefficient  $n_4$  includes all the contributions to the polarization proportional to  $E^5$  and is given by

$$n_4 = \frac{N}{n_0} \frac{\pi}{8} \chi_S^{(5)}(\omega). \quad (39)$$

Inserting the numerical value for  $\chi_S^{(5)}(\omega)$  given in Table IV we get  $n_4 = (-3.1 \times 10^{-40}) N \text{esu}$ . It is important to realize that  $n_4$  has a negative value and effectively reduces the nonlinear refractive index  $n_2$ . At an input intensity of  $1.5 \times 10^{11} \text{W/cm}^2$  the  $n_4$  term cancels exactly the  $n_2$  term and at higher intensities the total nonlinear refractive index  $n_2 + n_4 E^2$  becomes even negative, which leads to a defocusing of the incident beam.

For input powers  $W > W_{cr}$  a parallel light beam with an initial radius  $r_0$  is focused rather sharply after a length

$$z_{FP} = \frac{\sqrt{2}\pi r_0^2}{\lambda[(W/W_{cr})^{1/2} - 1]}. \quad (40)$$

This distance is modified in the case of a converging (or diverging) light wave by taking into account the negative (or positive) radius of curvature  $R$  of the wave front, yielding

$$z_F = z_{FP} R / (R - z_{FP}). \quad (41)$$

For our experimental conditions it turns out that in the case of the 300-psec pulses, self-focusing does not occur within the nonlinear medium up to the highest input powers ( $6 \times 10^7 \text{W}$ ) even if one neglects higher-order nonlinearities of the refractive index. This finding is in agreement with our experimental observations, which revealed no anomalous behavior of the output beam with respect to its intensity distribution and showed good agreement with theory up to the highest input intensities.

In the case of the 7-psec pulses, however, the threshold power for self-focusing within the Rb vapor zone of length  $L = 28 \text{cm}$  is calculated to be  $4.6 \times 10^7 \text{W}$  using Eq. (36) (this corresponds to an intensity of  $4 \times 10^{10} \text{W/cm}^2$ ). For the highest input powers ( $2.5 \times 10^8 \text{W}$ ) a self-focusing distance of 7 cm is estimated. This is in contrast to our experimental findings. Photographic recordings of the output pattern behind the heat pipe of the fundamental as well as the harmonic beam showed a smooth intensity distribution with the proper beam diameter even for the highest input powers. This strongly suggests that the self-focusing of the fundamental wave within the Rb vapor is suppressed by higher-order nonlinearities of the refractive index which have been neglected in the preceding estimate and tend to increase the criti-

TABLE IV. Fifth-order nonlinear susceptibilities (esu for the 5S ground state of Rb calculated for  $\lambda = 10\,600 \text{\AA}$  as defined by Eqs. (A5)–(A9).

$\chi^{(5)}(5\omega)$	$\chi_T^{(5)}(3\omega)$	$\chi_T^{(5)}(3\omega, \omega)$	$\chi_S^{(5)}(\omega)$	$\chi_S^{(5)}(3\omega)$	$\chi_S^{(5)}(3\omega, \omega)$	$\chi_S^{(5)}(\omega, 3\omega)$
$3.11 \times 10^{-43}$	$7.78 \times 10^{-42}$	$-1.20 \times 10^{-42}$	$-7.77 \times 10^{-40}$	$1.45 \times 10^{-41}$	$1.41 \times 10^{-41}$	$-9.50 \times 10^{-40}$

cal power  $W_{cr}$  and the distance of the focal point  $z_F$ .

At this stage it is interesting to go back to Fig. 6. Although we have no direct experimental evidence for focusing or defocusing of the incident light beam, we like to point out the following facts:

(i) A large scatter of the third-harmonic signal, which significantly exceeds the theoretical calculations, is observed at an input intensity in excess of  $2 \times 10^{10}$  W/cm<sup>2</sup>. This value is close to the theoretical value for the onset of self-focusing estimated above.

(ii) Our data appear to show a crossover with the theoretical curve at an input intensity of  $1.5 \times 10^{11}$  W/cm<sup>2</sup>. At this intensity our estimates indicate a cancellation of the nonlinear refractive indices ( $n_2 + n_4 E^2 = 0$ ) and hence no focusing or defocusing.

(iii) At the highest input intensities of  $2 \times 10^{11}$  W/cm<sup>2</sup> our measurements are below the theoretical curve which would be consistent with a defocusing due to the dominant negative  $n_4$  term.

From these observations we conclude that at very high input powers a quantitative evaluation of the third-harmonic intensity is no longer possible without taking into account explicitly the self-focusing process in Eqs. (29)–(31) by including the  $\Delta_{\perp}$  and the  $\nabla_{\perp}$  terms in Eq. (19).

#### E. Multiphoton ionization

In recent experiments of resonantly enhanced frequency mixing<sup>28</sup> it has been demonstrated that significant degrees of ionization may be obtained within the nonlinear medium. Such a process would lead to a depletion of the ground state of Rb and would affect the total nonlinear susceptibilities of the system. In our experiment transitions to the continuum via a four-photon ionization process have to be considered, since in this case one has an energy resonance of four photons and a free electron.

Miles and Harris<sup>2</sup> quoted an ionization probability of the ground state of Rb of  $W_0 \approx (10^{-32})\Phi^4 \text{ sec}^{-1}$ , calculated according to Morton,<sup>29</sup> where  $\Phi$  is given in W/cm<sup>2</sup>. Taking this value, we would expect a complete ionization of the irradiated Rb column in the case of the 300-psec pulses at input intensities larger than  $2 \times 10^{10}$  W/cm<sup>2</sup>. This estimate does not agree with our experimental observations, which show quite effective third-harmonic generation above this intensity level, whereas a complete depletion of the ground-state population during the laser pulse would reduce the third-harmonic generation considerably. Based on our experiments we are able to estimate an upper limit for the ionization probability of  $(10^{-35})\Phi^4 \text{ sec}^{-1}$ . This value

comes closer to an estimate based on the work of Keldysh,<sup>30</sup> where the probability of direct transitions from the ground state to the continuum is calculated, neglecting resonant contributions (the Rb atom shows no resonance closer than  $400 \text{ cm}^{-1}$ ). Following the work of Keldysh we estimate for the ground state 5S an ionization probability of  $W_0(5S) \approx (10^{-38})\Phi^4 \text{ sec}^{-1}$ . Hence, even for  $\Phi = 2 \times 10^{11}$  W/cm<sup>2</sup> the direct ionization of the 5S level is negligibly small.

Finally, it should be pointed out that for our experimental conditions an electrical breakdown of the medium due to avalanche ionization<sup>31</sup> is not very likely to occur, since the electron doubling time, during which an electron gathers energy from the light field via inverse bremsstrahlung and undergoes an inelastic ionizing collision, is typically of the order of 1 nsec. However, in the case of pulse durations in excess of 1 nsec and total pressures of the order of several 1000 Torr, this process may lead to an even lower ionization threshold than given by the multiphoton ionization process.

#### V. SUMMARY

Summarizing our investigations of the third-harmonic generation in Rb-Xe mixtures, some of the essential properties of a two-component system should be pointed out. Owing to the relatively small third-harmonic coefficient of Rb, input intensities in excess of typically  $10^{11}$  W/cm<sup>2</sup> at  $10\,600 \text{ \AA}$  are required in order to achieve energy-conversion efficiencies of a few percent. Our experiments have shown that at these intensity levels the third- and fifth-order nonlinear susceptibilities give rise to a change of the total refractive index of the system which affects the phase matching. Furthermore, self-focusing may occur. This problem cannot be avoided by operating the system at moderate input intensities and increasing the length and the particle density of the nonlinear medium, because in this case the phase-matching condition becomes stringent at lower input intensities. Model calculations have shown that the loss of the phase matching at high power levels can be compensated to some extent by properly adjusting the Rb-Xe pressure ratio.

So far, we have shown experimentally that an energy conversion up to 3% is possible. Our numerical results indicate that for an optimum Rb-Xe pressure ratio, energy-conversion efficiencies up to 10% should be feasible with our experimental parameters. A change to a larger length or pressure of the nonlinear medium would alter the phase-matching conditions significantly and new

calculations of the energy conversion have to be performed. Calculations of this kind which would reveal the optimum experimental parameters are in progress. Their results will be reported in a later paper.

#### APPENDIX: EXTENSION TO FIFTH ORDER

At very large incident electromagnetic fields the question arises whether or not higher-order nonlinearities become important for the third-harmonic generation. For this purpose an extension of Eqs. (29)–(31) including the fifth-order nonlinear susceptibilities is presented. For our experimental conditions the extended equations have been evaluated numerically in order to demonstrate the convergence of our calculations. The fifth order of the perturbation gives rise to the following additional contributions to the nonlinear polarizations,  $\vec{P}_q^r$  and  $\vec{P}_q^s$ :

$$\begin{aligned} \vec{P}_1^r = & \frac{1}{16} N [\chi^{(5)}(\omega = 3\omega - \omega - \omega - \omega + \omega) |\vec{E}_1|^2 \vec{E}_3 (\vec{E}_1^*)^2 \\ & + \chi^{(5)}(\omega = 3\omega + 3\omega - 3\omega - \omega - \omega) |\vec{E}_3|^2 \vec{E}_3 (\vec{E}_1^*)^2 \\ & + \chi^{(5)}(\omega = \omega + \omega + \omega + \omega - 3\omega) (\vec{E}_1^*)^4 \vec{E}_3^*], \end{aligned} \quad (\text{A1})$$

$$\begin{aligned} \vec{P}_3^r = & \frac{1}{16} N [\chi^{(5)}(3\omega = \omega + \omega + \omega + \omega - \omega) |\vec{E}_1|^2 (\vec{E}_1^*)^3 \\ & + \chi^{(5)}(3\omega = 3\omega - 3\omega + \omega + \omega) |\vec{E}_3|^2 (\vec{E}_1^*)^3 \\ & + \chi^{(5)}(3\omega = 3\omega + 3\omega - \omega - \omega - \omega) (\vec{E}_3^*)^2 (\vec{E}_1^*)^3], \end{aligned} \quad (\text{A2})$$

$$\begin{aligned} \vec{P}_1^s = & \frac{1}{16} N [\chi^{(5)}(\omega = \omega + \omega + \omega - \omega - \omega) |\vec{E}_1|^4 \vec{E}_1 \\ & + \chi^{(5)}(\omega = 3\omega + 3\omega - 3\omega - 3\omega + \omega) |\vec{E}_3|^4 \vec{E}_1 \\ & + \chi^{(5)}(\omega = 3\omega - 3\omega + \omega - \omega + \omega) |\vec{E}_3|^2 |\vec{E}_1|^2 \vec{E}_1], \end{aligned} \quad (\text{A3})$$

$$\begin{aligned} \vec{P}_3^s = & \frac{1}{16} N [\chi^{(5)}(3\omega = 3\omega + \omega - \omega + \omega - \omega) \vec{E}_3 |E_1|^4 \\ & + \chi^{(5)}(3\omega = 3\omega + 3\omega - 3\omega + 3\omega - 3\omega) |\vec{E}_3|^4 \vec{E}_3 \\ & + \chi^{(5)}(3\omega = 3\omega + 3\omega - 3\omega + \omega - \omega) |\vec{E}_3|^2 \vec{E}_3 |\vec{E}_1|^2]. \end{aligned} \quad (\text{A4})$$

From symmetry considerations these 12 nonlinear susceptibilities may be reduced to a set of six independent coefficients which will be abbreviated as follows:

$$\begin{aligned} \chi_T^{(5)}(3\omega) & \equiv \chi^{(5)}(3\omega = \omega + \omega + \omega + \omega - \omega) \\ & = \chi^{(5)}(\omega = \omega + \omega + \omega + \omega - 3\omega) \\ & = \frac{1}{4} \chi^{(5)}(\omega = 3\omega - \omega - \omega - \omega + \omega), \end{aligned} \quad (\text{A5})$$

$$\begin{aligned} \chi_T^{(5)}(3\omega, \omega) & \equiv \chi^{(5)}(3\omega = 3\omega + 3\omega - \omega - \omega - \omega) \\ & = \frac{1}{2} \chi^{(5)}(3\omega = 3\omega - 3\omega + \omega + \omega) \\ & = \frac{1}{3} \chi^{(5)}(\omega = 3\omega + 3\omega - 3\omega - \omega - \omega), \end{aligned} \quad (\text{A6})$$

$$\chi_S^{(5)}(q\omega) \equiv \chi^{(5)}(q\omega = q\omega + q\omega + q\omega - q\omega - q\omega), \quad (\text{A7})$$

with  $q = 1$  and  $q = 3$ ,

$$\begin{aligned} \chi_S^{(5)}(3\omega, \omega) & \equiv \chi^{(5)}(3\omega = 3\omega + \omega - \omega - \omega) \\ & = \frac{1}{2} \chi^{(5)}(\omega = 3\omega - 3\omega + \omega - \omega + \omega), \end{aligned} \quad (\text{A8})$$

$$\begin{aligned} \chi_S^{(5)}(\omega, 3\omega) & \equiv \chi^{(5)}(\omega = \omega + 3\omega - 3\omega + 3\omega - 3\omega) \\ & = \frac{1}{2} \chi^{(5)}(3\omega = 3\omega + 3\omega - 3\omega + \omega - \omega). \end{aligned} \quad (\text{A9})$$

For the Nd:glass laser frequency ( $\lambda = 1.06 \mu\text{m}$ ) numerical values of these susceptibilities are presented in Table IV. They were calculated using the recursion relations given in Ref. 9. In addition to the reduced dipole-moment matrix elements tabulated by Eicher<sup>11</sup> we included in our calculations the matrix elements for the  $nD-n'F$  transitions with  $4 \leq n \leq 18$  and  $4 \leq n' \leq 8$ . These values (tabulated in Table V) were kindly provided by Eicher and have been obtained by the same procedure as described in Ref. 11.

In order to show that the process of fifth-harmonic generation,  $P(5\omega) \sim \chi^{(5)}(5\omega)E_1^5$ , can be neglected, Table IV contains also the numerical value of the corresponding nonlinear susceptibility  $\chi^{(5)}(5\omega)$ . It is almost two orders of magnitude smaller than the fifth-order coefficient for the third-harmonic generation,  $\chi_T^{(5)}(3\omega)$ . With regard to the intensity-dependent refractive index the major modification in fifth order arises from the  $\chi_S^{(5)}(\omega)$  coefficient. Note that the  $\chi_S^{(5)}(\omega)$  has the opposite sign with respect to  $\chi_S^{(3)}(\omega)$ . Hence, at large incident intensities the intensity-dependent refractive index associated with  $\chi_S^{(3)}(\omega)$  is compensated by the corresponding fifth-order term. At incident intensities in excess of  $1.5 \times 10^{11} \text{ W/cm}^2$  the fifth-order term even dominates, as pointed out in Sec. IV D.

TABLE V. Reduced dipole matrix elements for the  $nD-n'F$  transitions in Rb given in atomic units.

	4F	5F	6F	7F	8F
4D	-6.306	-2.845	-1.751	-1.239	-0.947
5D	15.788	-5.9	-3.25	-2.153	-1.58
6D	-5.892	29.37	-5.553	-3.412	-2.356
7D	-1.500	-12.44	45	-5.264	-3.523
8D	-0.765	-3.09	-20.65	63.05	-4.959
9D	-0.491	-1.554	-5.035	-30.56	83.732
10D	-0.354	-0.994	-2.519	-42.262	-42.147
11D	-0.273	-0.713	-1.6	-3.653	-3.169
12D	-0.220	-0.548	-1.145	-2.312	-4.948
13D	-0.183	-0.441	-0.878	-1.645	-3.119
14D	-0.156	-0.368	-0.706	-1.261	-2.214
15D	-0.135	-0.313	-0.586	-1.01	-1.692
16D	-0.119	-0.271	-0.499	-0.839	-1.362
17D	-0.105	-0.237	-0.431	-0.713	-1.115
18D	-0.095	-0.212	-0.38	-0.618	-0.952

Here we should note that the numerical values of the fifth-order nonlinear susceptibilities tabulated in Table IV include the contributions due to transient one-photon and two-photon excitations (adiabatic following), which become important in the transient time domain  $\tau \ll T_1$ , as demonstrated in Ref. 9. Furthermore, the perturbation approach for evaluating the nonlinear polarizations covers also the lowest-order contributions of the energy-level shifts due to the ac Stark effect.

Inserting Eqs. (A1)–(A4) into Eq. (19) and sepa-

rating the resulting set of equations into their real and imaginary parts we obtain a set of equations similar to Eqs. (29)–(31) which now include all the third- and fifth-order contributions. With

$$B_T = \chi_T^{(3)}(3\omega) + \chi_T^{(5)}(3\omega)\rho_1^2 G_1^2 / 4F \\ + \chi_T^{(5)}(3\omega, \omega)\rho_3^2 G_3^2 / 4F, \quad (\text{A10})$$

which may be interpreted as the field-dependent third-harmonic coefficient, we have

$$\frac{d\rho_1}{dz} = \frac{-3\pi\omega N}{2n_1 cF} B_T \rho_1^2 \rho_3 G_1 G_3 \sin\Theta, \quad (\text{A11})$$

$$\frac{d\rho_3}{dz} = \frac{3\pi\omega N}{2n_3 cF} B_T \rho_1^3 \frac{G_1^3}{G_3} \sin\Theta, \quad (\text{A12})$$

$$\frac{d\Theta}{dz} = \frac{4}{\hbar F} - \Delta k(z) + \frac{3\pi\omega N}{2n_1 cF} \rho_1 \rho_3 G_1 G_3 \left[ \left( \frac{n_1 G_1^2 \rho_1^2}{n_3 G_3^2 \rho_3^2} - 3 \right) B_T + \frac{1}{2} \frac{\rho_1^2 G_1^2}{F} \left( \frac{n_1}{n_3} \chi_T^{(5)}(3\omega, \omega) - \chi_T^{(5)}(3\omega) \right) \right] \cos\Theta \\ + \frac{3\pi\omega N}{2n_1 cF} \left[ \rho_1^2 G_1^2 \left( \frac{n_1}{n_3} \chi_S^{(3)}(\omega, 3\omega) - \chi_S^{(3)}(\omega) \right) + \rho_3^2 G_3^2 \left( \frac{n_1}{n_3} \chi_S^{(3)}(3\omega) - \chi_S^{(3)}(\omega, 3\omega) \right) + \frac{\rho_1^4 G_1^4}{4F} \left( \frac{n_1}{n_3} \chi_S^{(5)}(3\omega, \omega) - \chi_S^{(5)}(\omega) \right) \right. \\ \left. + \frac{\rho_3^4 G_3^4}{4F} \left( \frac{n_1}{n_3} \chi_S^{(5)}(3\omega) - \chi_S^{(5)}(\omega, 3\omega) \right) + \frac{\rho_1^2 G_1^2 \rho_3^2 G_3^2}{8F} \left( \frac{n_1}{n_3} \chi_S^{(5)}(\omega, 3\omega) - \chi_S^{(5)}(3\omega, \omega) \right) \right]. \quad (\text{A13})$$

All nonlinear susceptibilities are assumed to be real quantities. The first three terms of Eq. (A13) represent the phase shifts associated with the focusing, the wave-vector mismatch, and the third-harmonic generation process, respectively. The remaining part describes the phase shift due to the intensity-dependent refractive indices

created by the fundamental and the harmonic waves. For practical purposes Eqs. (A11)–(A13) may be simplified by neglecting all terms proportional to the second and higher powers of  $\rho_3$  as long as the conversion efficiency is below typically 20%. In our numerical integration of Eqs. (A11)–(A13), however, we retained all terms.

- \*Present address: Max-Planck-Institut für Extraterrestrische Physik, Garching, Germany.
- <sup>1</sup>S. E. Harris and R. B. Miles, *Appl. Phys. Lett.* **19**, 385 (1971).
- <sup>2</sup>R. B. Miles and S. E. Harris, *IEEE J. Quantum Electron.* **QE-9**, 470 (1973).
- <sup>3</sup>J. F. Young, G. C. Bjorklund, A. H. Kung, R. B. Miles, and S. E. Harris, *Phys. Rev. Lett.* **27**, 1551 (1971).
- <sup>4</sup>A. H. Kung, J. F. Young, G. C. Bjorklund, and S. E. Harris, *Phys. Rev. Lett.* **29**, 985 (1972).
- <sup>5</sup>R. T. Hodgson, P. R. Sorokin, and J. J. Wynne, *Phys. Rev. Lett.* **32**, 343 (1974).
- <sup>6</sup>A. H. Kung, *Appl. Phys. Lett.* **25**, 653 (1974).
- <sup>7</sup>D. M. Bloom, G. W. Bekkers, J. F. Young, and S. E. Harris, *Appl. Phys. Lett.* **26**, 687 (1975).
- <sup>8</sup>H. Puell and C. R. Vidal, *Laser Spectroscopy, Proceedings of the Second International Conference, Megève, 1975*, edited by S. Haroche, J. C. Pebay-Peyroula, T. W. Hänsch, and S. E. Harris (Springer, Berlin, 1975), p. 461.
- <sup>9</sup>H. Puell and C. R. Vidal, preceding paper, *Phys. Rev. A* **14**, 2225 (1976).
- <sup>10</sup>J. A. Armstrong, N. Bloembergen, J. Ducuing, and

- P. S. Pershan, *Phys. Rev.* **127**, 1918 (1962).
- <sup>11</sup>H. Eicher, *IEEE J. Quantum Electron.* **QE-11**, 121 (1973).
- <sup>12</sup>The value of the reduced dipole-moment matrix element for the resonant transition  $5S-5P$  was reduced by 1% from  $-5.31$  to  $-5.25$  because of reasons to be discussed in Sec. IV.
- <sup>13</sup>It will be shown below that the generated third harmonic is also a Gaussian beam with the same confocal parameters as the fundamental beam. This is true for all sum-frequency processes (at least at moderate conversions), but does not hold for difference-frequency mixing processes. See Ref. 17.
- <sup>14</sup>H. Kogelnik and T. Li, *Appl. Opt.* **5**, 1550 (1966).
- <sup>15</sup>S. A. Akhmanov, R. V. Khokhlov, and A. P. Sukhorukov, *Laser Handbook*, edited by F. T. Arecchi and E. O. Schulz-Dubois (North-Holland, Amsterdam, 1972), Vol. 2, p. 1088.
- <sup>16</sup>J. F. Ward and G. H. New, *Phys. Rev.* **185**, 57 (1969).
- <sup>17</sup>G. C. Bjorklund, *IEEE J. Quantum Electron.* **QE-11**, 287 (1975).
- <sup>18</sup>J. A. Giordmaine, *Phys. Rev. Lett.* **8**, 19 (1962); P. D. Maker, R. W. Terhune, M. Nisenoff, and C. M. Savage,

- Phys. Rev. Lett. 8, 21 (1962).
- <sup>19</sup>P. P. Bey, J. F. Guiliani, and H. Rabin, Phys. Rev. Lett. 19, 819 (1967).
- <sup>20</sup>J. Koch, in *Landolt-Börnstein, Zahlenwerte und Funktionen aus Physik*, edited by K. H. Hellwege and A. M. Hellwege (Springer, Berlin, 1962), Vol. 2/8, p. 6-885.
- <sup>21</sup>C. R. Vidal and F. B. Haller, Rev. Sci. Instrum. 42, 1779 (1971).
- <sup>22</sup>C. R. Vidal and J. Cooper, J. Appl. Phys. 40, 3370 (1969).
- <sup>23</sup>D. von der Linde, O. Bernecker, and A. Laubereau, Opt. Commun. 2, 215 (1970).
- <sup>24</sup>J. A. Giordmaine, P. M. Rentzepis, S. L. Shapiro, and K. W. Wecht, Appl. Phys. Lett. 11, 216 (1967).
- <sup>25</sup>A. Penzkofer, D. von der Linde, and A. Laubereau, Opt. Commun. 4, 377 (1972).
- <sup>26</sup>E. M. Anderson and V. A. Zilitis, Opt. Spectrosc. 16, 211 (1964).
- <sup>27</sup>P. P. Sorokin and J. R. Lankard, IEEE J. Quantum Electron. QE-9, 227 (1973).
- <sup>28</sup>P. P. Sorokin, J. J. Wynne, J. A. Armstrong, and R. T. Hodgson, Ann. N.Y. Acad. Sci. 267, 30 (1976).
- <sup>29</sup>V. M. Morton, Proc. Phys. Soc. Lond. 92, 301 (1967).
- <sup>30</sup>L. V. Keldysh, Sov. Phys.-JETP 20, 1307 (1965).
- <sup>31</sup>Yu. P. Raizer, Sov. Phys.-Usp. 8, 650 (1966).